J. Fluid Mech. (1999), *vol.* 392, *pp.* 361–377. Printed in the United Kingdom

The second-law analysis of convective pattern change in a rectangular cavity

By UICHIRO NARUSAWA

MIME Department (Department of Mechanical, Industrial and Manufacturing Engineering), Northeastern University, Boston, MA 02115, USA

(Received 21 August 1996 and in revised form 22 February 1999)

Natural convection in a rectangular cavity is examined, utilizing the second law of thermodynamics. Through an application of the second law the rate of entropy generation associated with the convective pattern changes is evaluated for the onset of natural convection in a cavity with free boundaries, for which an exact solution is sought, as well as with rigid boundaries which is studied numerically. Entropy to be generated from the perturbed temperature and velocity fields is shown to depend on AR (aspect ratio of the cavity), Ra_c (the critical Rayleigh number) and a non-dimensional parameter, Ω, which is related to the ratio of entropy generation by viscous friction to that by thermal transport. The convective pattern change is related to a change in the spatial distributions of the rate of entropy generation due to heat transfer and due to dissipation, demonstrating that an application of the second law helps examine convective pattern changes quantitatively by dealing with temperature and velocity fields in a unified manner.

1. Introduction

The effects of buoyancy-induced flow have been studied extensively in the past because of its various scientific and engineering applications (Turner 1973; Gebhart *et al.* 1988). In many engineering fields an understanding of the details of flow and thermal structures is increasingly becoming important due to more stringent requirements in optimal design of equipment as well as in new processing technology. Also, analyses of simpler systems are useful to understand some important features of complex pattern forming processes in various fields including physics, chemistry, biology and social systems. Because of the relative ease with which quantitative comparisons may be made between theory and experiment, thermal convection has been investigated widely to gain insights into processes of pattern (organized structures) formation (Zimmermann 1991).

The engineering utilization of the second law, known as availability (exergy) analysis, had been a major part of thermodynamic analysis of industrial equipment, particularly in power industries. More recently the second-law analysis focusing on entropy generation and its minimization has been applied to transport processes to optimize thermal insulation and heat transfer augmentation systems as well as heat exchangers. The second law has also been used to understand the structural development of turbulence (Bejan 1982).

The linear stability of the onset of natural convection in a cavity heated at the bottom and cooled at the top with adiabatic sidewalls has been studied (Kurzweg 1965; Davis 1967). Unlike the case of a fluid layer between two horizontal boundaries

the presence of vertical boundaries not only increases the critical Rayleigh number for the onset of convective motion, but also causes changes in the number of convective rolls that develop as the width of the cavity is varied. For example, for a two-dimensional cavity with rigid boundaries Kurzweg showed the transitions in the number of convective rolls to occur at the following aspect ratios AR (width/height of the cavity): 1.6 for one to two rolls, 2.7 for two to three rolls, 3.7 for three to four rolls.

In this report a linear stability analysis which predicts transitions in the number of convective rolls that develop at the critical conditions is combined with the second law of thermodynamics to study convective pattern changes in a low aspect ratio cavity in terms of the entropy generation. After a general theoretical development of entropy generation due to natural convection in a rectangular cavity the paper discusses the stability of a fluid in a two-dimensional rectangular cavity heated at the bottom with the free (impermeable, zero shear) boundary condition imposed at the four boundaries. The study of a more realistic non-slip (rigid) boundary condition, reported in § 4, involves a more complex mathematical analysis requiring a numerical approach.

2. General formulation of entropy generation due to natural convection in a cavity

Consider a rectangular cavity of width W and height H with the origin of a coordinate system x and y located at the centre of the cavity, and the direction of gravity, g, in the negative y-direction. Temperatures at the bottom and the top are kept at T_1 and $T_2 (< T_1)$ respectively with $\Delta T = T_1 - T_2$; the side boundaries are adiabatic. For a steady, incompressible natural convective flow, employing the Boussinesq approximation with a linearized equation of state, non-dimensional governing equations with constant thermophysical properties may be written as

$$\frac{AR}{Pr}\frac{\mathrm{D}}{\mathrm{D}t}(\nabla^2\Psi) = \nabla^4\Psi - \left(\frac{AR}{2}\right)^4 Ra\,\frac{\partial\theta}{\partial x}, \tag{1a}$$

$$AR\,\frac{\mathrm{D}\theta}{\mathrm{D}t} = \nabla^2\theta - \frac{\partial\Psi}{\partial x}, \tag{1b}$$

where AR (aspect ratio) $= W/H$, Pr (Prandtl number) $= \nu/D_T$, Ra (Rayleigh number) $= g\alpha\Delta T\,H^3/\nu\,D_T$, $\mathrm{D}/\mathrm{D}t = u\,\partial/\partial x + v\,\partial/\partial y$, $\nabla^2 = \partial^2/\partial x^2 + AR^2\,\partial^2/\partial y^2$ with ν the kinematic viscosity, D_T the thermal diffusivity, α the thermal expansion coefficient. Dimensional coordinates, (x', y'), velocity (u', v') and temperature, T, are related to the corresponding non-dimensional variables as

$$(x, y) = \left(\frac{x'}{W/2}, \frac{y'}{H/2}\right), \qquad \Psi(\text{stream function}) = \Psi'/D_T,$$

$$\boldsymbol{V} = u\hat{\boldsymbol{i}} + v\hat{\boldsymbol{j}} = \frac{2D_T}{H}\frac{\partial\Psi}{\partial y}\hat{\boldsymbol{i}} - \frac{2D_T}{W}\frac{\partial\Psi}{\partial x}\hat{\boldsymbol{j}}, \qquad \theta = \frac{T - T_0(y)}{\frac{1}{2}AR\,\Delta T},$$

with $T_0(y) = (T_1 + T_2)/2 - \Delta T\,y/2$ the temperature distribution of the base conduction state. The boundary conditions are: if the boundaries are free

$$\Psi = \frac{\partial^2\Psi}{\partial x^2} = \frac{\partial\theta}{\partial x} = 0 \ \text{ at } \ x = \pm 1, \qquad \Psi = \frac{\partial^2\Psi}{\partial y^2} = \theta = 0 \ \text{ at } \ y = \pm 1; \tag{2a}$$

if the boundaries are rigid

$$\Psi = \frac{\partial \Psi}{\partial x} = \frac{\partial \theta}{\partial x} = 0 \ \text{ at } \ x = \pm 1, \qquad \Psi = \frac{\partial \Psi}{\partial y} = \theta = 0 \ \text{ at } y = \pm 1. \tag{2b}$$

The local volumetric rate of entropy generation, S'''_G [W m^{-3} K^{-1}], based on the second law of thermodynamics, is

$$S'''_G = \frac{k}{T^2}\left(\left(\frac{\partial T}{\partial x'}\right)^2 + \left(\frac{\partial T}{\partial y'}\right)^2\right) + \frac{\mu}{T}\left(2\left(\left(\frac{\partial u'}{\partial x'}\right)^2 + \left(\frac{\partial v'}{\partial y'}\right)^2\right) + \left(\frac{\partial u'}{\partial y'} + \frac{\partial v'}{\partial x'}\right)^2\right), \tag{3a}$$

where k is thermal conductivity, μ is viscosity (Bejan). The first term on the right-hand side is due to heat transfer ($= S'''_{GH}$) and the second term is due to viscous dissipation ($= S'''_{GV}$). It is well known that the viscous dissipation in the first law of thermodynamics is negligible in many applications. The ratio, S'''_{GV} / S'''_{GH}, becomes $(T_R/\Delta T_R)\, R_I$ where R_I is the ratio of viscous dissipation to conduction in the first law with T_R and ΔT_R indicating the characteristic scales. Hence, even if the dissipation is negligible in the first law (which is the case in the present study), it may be important in the second law due to the presence of the factor, $(T_R/\Delta T_R)$. In terms of non-dimensional variables (3a) may be expressed as

$$S'''_G = S'''_{GH} + S'''_{GV}, \tag{3b}$$

where

$$S'''_{GH} = k\left(\frac{\Delta T}{H\,T}\right)^2\left(\left(\frac{\partial \theta}{\partial x}\right)^2 + \left(AR\frac{\partial \theta}{\partial y} - 1\right)^2\right),$$

$$S'''_{GV} = \frac{\mu}{T}\left(\frac{4\,D_T}{W^2}\right)^2\left(4\,AR^2\left(\frac{\partial^2 \Psi}{\partial x \partial y}\right)^2 + \left(AR^2\frac{\partial^2 \Psi}{\partial y^2} - \frac{\partial^2 \Psi}{\partial x^2}\right)^2\right).$$

To find the total rate of entropy generation, S'_G [W m^{-1} K^{-1}], (3b) is integrated over the cavity, yielding

$$S'_G = \int_{-H/2}^{H/2}\int_{-W/2}^{W/2} S'''_G \,\mathrm{d}x'\,\mathrm{d}y' = S'_{GB} + S'_{GD}$$

$$= k\left(\frac{\Delta T}{T}\right)^2 AR + \frac{k}{4}\left(\frac{\Delta T}{T}\right)^2 AR\left(1 + Ra\,\frac{T}{\Delta T}\,\frac{\mu (D_T/H)^2}{k\Delta T}\right)\left\langle \theta\left(-\frac{\partial \Psi}{\partial x}\right)\right\rangle, \tag{4a}$$

with $\langle f \rangle = \int_{-1}^{1}\int_{-1}^{1} f \,\mathrm{d}x\,\mathrm{d}y$.

Or, by eliminating ΔT in favour of Ra,

$$\overline{S_G} = Ra^2\, AR + \tfrac{1}{4}(Ra^2 + \Omega\, Ra) AR\left\langle \theta\left(-\frac{\partial \Psi}{\partial x}\right)\right\rangle, \tag{4b}$$

where

$$\overline{S_G} = \frac{S'_G}{\Gamma}, \qquad \Gamma = k\left(\frac{\nu D_T}{\alpha g\, T\, H^3}\right)^2, \qquad \Omega = \frac{\rho(\alpha g H^2)^2\, T}{\nu k}.$$

In (4a) and (4b), the first term S_{GB} is due to base conduction. Since ΔT is directly related to Ra, S_{GB} increases linearly with the width W and with Ra^2 for a given fluid and a fixed value of height H. On the other hand, the second term, S_{GD},

due to perturbed thermofluid fields consists of contributions from heat transfer and viscous friction with the factor $Ra\,(T/\Delta T)[\mu(D_T/H)^2/(k\Delta T)]$ (or Ω/Ra) indicating the relative contributions of the two. This corresponds to the irreversibility distribution ratio (Bejan), defined for the perturbation field in the present context. As stated earlier, (4*a*) shows that even if the ratio of viscous dissipation to thermal diffusion, $\mu(D_T/H)^2/(k\Delta T)$, is negligible in the conservation of energy the presence of the additional factor, $T/\Delta T$ in Ω/Ra, makes it necessary to include the irreversibility associated with the viscous friction in our consideration of the second law, and that the first-order perturbation fields, Ψ and θ, linearized in the conservations of momentum and energy, appear as a product, $\theta(-\partial\Psi/\partial x)$, in the second law with $\langle\theta(-\partial\Psi/\partial x)\rangle$ representing the net vertical advection of thermal energy.

It should be emphasized here that all equations presented above are applicable for natural convection in a rectangular cavity with either free or rigid boundaries.

3. Onset of instability in a cavity with free boundaries

In a linear stability analysis the advective terms on the left-hand side of (1) may be neglected as second-order terms. Two possible solutions to the formulation: one for the onset of an odd number of convective rolls (to be referred to as the 'odd' solution), and the other for the onset of an even number of convective rolls (to be referred to as the 'even' solution) may be directly written as follows:
For the odd solution,

$$\Psi = A_o \cos(\tfrac{1}{2}\pi\hat{k}x)\cos(\tfrac{1}{2}\pi y), \qquad \theta = B_o \sin(\tfrac{1}{2}\pi\hat{k}x)\cos(\tfrac{1}{2}\pi y), \tag{5a}$$

For the even solution,

$$\Psi = A_e \sin(\tfrac{1}{2}\pi\hat{l}x)\cos(\tfrac{1}{2}\pi y), \qquad \theta = B_e \cos(\tfrac{1}{2}\pi\hat{l}x)\cos(\tfrac{1}{2}\pi y), \tag{5b}$$

where $\hat{k}$ and $\hat{l}$ are the number of rolls present in the cavity, i.e. $\hat{k} = 1, 3, 5, \ldots, \hat{l} = 2, 4, 6, \ldots$.

Then the critical Rayleigh number Ra_c as well as a relationship between $A_o(e)$ and $B_o(e)$ may be obtained as

$$Ra_c = \left(\frac{\pi}{AR}\right)^4 \frac{(\hat{M}^2 + AR^2)^3}{\hat{M}^2}, \tag{6a}$$

$$A_o = \frac{\pi}{2}\frac{\hat{k}^2 + AR^2}{\hat{k}}\,B_o, \qquad A_e = -\frac{\pi}{2}\frac{\hat{l}^2 + AR^2}{\hat{l}}\,B_e, \tag{6b}$$

where $\hat{M} = \hat{k}$ for the odd solution and $\hat{l}$ for the even solution. Equation (6*a*) is plotted in figure 1 as Ra_c versus AR. Of the two values of Ra_c at a specified value of AR, the lower of the two is the true Ra_c. Minima of Ra_c, $Ra_{c,min}$, occur at

$$AR_{min} = AR\,(Ra_c = RA_{c,min}) = \sqrt{2}\,\hat{M}. \tag{7}$$

At AR_{min} the critical horizontal wavenumber is $\sqrt{2}\,H$ and $Ra_{c,min}$ is equal to $27\pi^4/4\,(\sim 657.5)$; the same conditions as the onset of convective rolls between two horizontal boundaries (the Rayleigh–Bénard convection with free boundaries) (Turner). As AR increases the magnitude of Ra_c becomes insensitive to AR, rapidly approaching the value of $27\pi^4/4$. The aspect ratio, AR_{tran}, where changes in the number of convective rolls (from even (odd) to odd (even)) occur, may be obtained

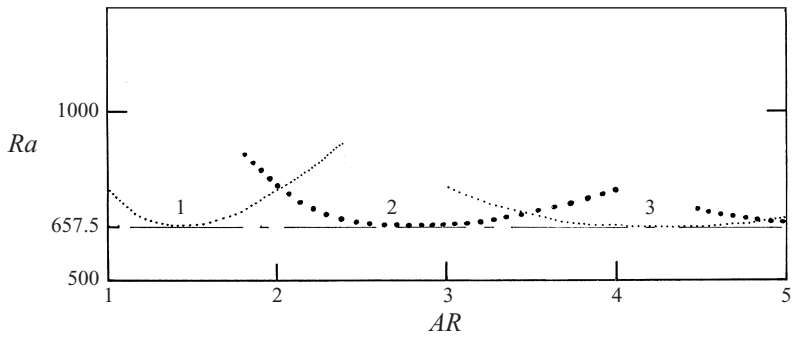

FIGURE 1. Linear stability in a cavity with free boundaries. Numbers above the curve represent the number of rolls in the cavity.

from (6*a*) as

$$\hat{k}^2 + AR_{tran}^2 = \left(\frac{\hat{k}}{\hat{l}}\right)^{2/3} (\hat{l}^2 + AR_{tran}^2). \tag{8}$$

These transitions occur at $AR_{tran} \approx 2.027$ (from one to two rolls), ~ 3.480 (from two to three), ~ 4.910 (from three to four) and ~ 9.006 (from four to five). Since the free, adiabatic side boundaries provide the same conditions as those at the interface between two neighbouring rolls, convective rolls at any given value of AR are identical in size to each other.

Based on (5), the total rate of entropy generation per depth, $\overline{S_G}$, in (4*b*) may be readily evaluated to yield

$$\overline{S_G} = Ra_c^2\, AR + \tfrac{1}{4}(Ra_c^2 + \Omega\, Ra_c) AR\Phi, \tag{9}$$

with

$$\Phi = \begin{cases} \frac{1}{2}\pi A_o\, B_o\, \hat{k} = \left(\frac{1}{2}\pi\right)^2 (\hat{k}^2 + AR^2) B_o^2 & \text{for odd solutions} \\ -\frac{1}{2}\pi A_e\, B_e\, \hat{l} = \left(\frac{1}{2}\pi\right)^2 (\hat{l}^2 + AR^2) B_e^2 & \text{for even solutions.} \end{cases}$$

Equation (6*b*) is used to derive the second expression of Φ. The coefficients, B_o, B_e, in Φ remain indeterminate as a solution to the characteristic equation constructed from conservation of momentum (or the vorticity equation) and conservation of energy. However, in order to compare the magnitudes of the rate of entropy generation between the odd and the even solutions, a relationship between the two coefficients must be specified with respect to the second law. The required condition is that at the transition between an odd and an even number of rolls (i.e. at $Ra_{c\,(odd)} = Ra_{c\,(even)}$), the magnitude of $\overline{S_G}$, as a measure of irreversibility associated with both heat transfer and viscous dissipation, is the same between the two solutions so that the selection between the two convective pattern is equally likely. The condition also implies that a net vertical advection of perturbed thermal energy is the same between the odd and the even solutions for quantitative comparisons. Furthermore, as has been mentioned earlier in relation to (7), convective rolls at AR_{min} are identical to the ones between two horizontal boundaries (without side boundaries); therefore, at $AR_{min} = \sqrt{2}\,\hat{M}$, the rate of entropy generation per roll must be constant, independent of the number of rolls, $\hat{M}$. This is also satisfied by the imposed condition, as shown below.

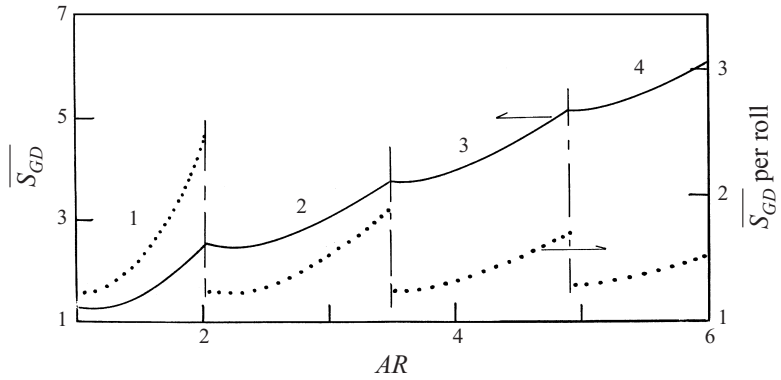

FIGURE 2. $\overline{S_{GD}}$ (solid) and $\overline{S_{GD}}$ per roll (dotted) vs. AR for $\Omega = 100$ (free boundaries). Numbers above the curve represent the number of rolls in the cavity.

For fixed values of Γ and Ω, (9) implies that the condition is satisfied if

$$(\hat{k}^2 + AR^2)B_o^2 = (\hat{l}^2 + AR^2)B_e^2. \tag{10}$$

From (6*b*) and (10), $A_{o(e)}$ and $B_{o(e)}$ become

$$A_o = C'\left(\tfrac{1}{2}\pi\right)\frac{(\hat{k}^2 + AR^2)^{1/2}}{\hat{k}}, \qquad B_o = \frac{C'}{(\hat{k}^2 + AR^2)^{1/2}}, \tag{11a}$$

$$A_e = C'\left(\tfrac{1}{2}\pi\right)\frac{(\hat{l}^2 + AR^2)^{1/2}}{\hat{l}}, \qquad B_e = \frac{C'}{(\hat{l}^2 + AR^2)^{1/2}}, \tag{11b}$$

with $C' =$ arbitrary constant. Then, we obtain the rate of entropy generation due to perturbed thermofluid fields, S_{GD}, as

$$S_{GD} = \left(\frac{\pi^2}{16}\right) C'^2\,\Gamma\,(Ra_c^2 + \Omega\,Ra_c)AR. \tag{12}$$

Also,

$$S_{GB} \text{ per roll at } AR_{min} = \sqrt{2}\,C'^2\,\Gamma\,Ra_c^2, \tag{13a}$$

$$S_{GD} \text{ per roll at } AR_{min} = \frac{\sqrt{2}\,\pi^2}{16}\,C'^2\,\Gamma\,(Ra_c^2 + \Omega\,Ra_c). \tag{13b}$$

It should be mentioned that (10) holds only at $AR = AR_{tran}$; however, $A_{o(e)}$ and $B_{o(e)}$, of (11) are valid for $AR \neq AR_{tran}$.

Given fluid properties, the temperature level $T(=(T_1+T_2)/2)$ and the cavity height, H, the non-dimensional parameters Γ and Ω are fixed with the relative importance of heat transfer and viscous friction being proportional to Ra_c^2 and Ra_c, respectively, and with Ω/Ra_c indicating the ratio of entropy production due to viscous friction to that due to heat transfer. If we select the temperature level, $T \sim 300$ K and the cavity height $H \sim 0.1$ m, Ω has an order of magnitude of ~ 100 with $\Omega/Ra_c \sim 0.1$ for air as an ideal gas; on the other hand, for liquid water, $\Omega \sim 500$, $\Omega/Ra_c \sim 0.5$ with $\Omega_{liquid}/\Omega_{gas} \sim 5$, indicating that at the critical condition in a cavity with $H \sim 0.1$ m, the entropy generation for gases is mostly due to the perturbed temperature field.

In figure 2 a non-dimensional rate of entropy generation due to perturbed thermo-

fluid fields, $\overline{S_{GD}}$ (solid), is plotted against AR for $\Omega = 100$. $\overline{S_{GD}}$ is defined as

$$\overline{S_{GD}} = \frac{S_{GD}}{\frac{1}{16}\pi^2 C'^2 \Gamma\,((\frac{27}{4}\pi^4)^2 + \Omega(\frac{27}{4}\pi^4))} = \frac{Ra_c^2 + \Omega\, Ra_c}{\left((\frac{27}{4}\pi^4)^2 + \Omega(\frac{27}{4}\pi^4)\right)} AR. \tag{14}$$

The factor, $((\frac{27}{4}\pi^4)^2 + \Omega(\frac{27}{4}\pi^4))$, corresponds to $(Ra_c^2 + \Omega\, Ra_c)$ evaluated for a fluid between two horizontal boundaries as $AR \to \infty$. Given the type of fluid, the temperature level T and the cavity height H, the figure represents the increase in S_{GD} as the width of the cavity changes. It is similar to Ra_c versus AR of figure 1 because of a direct relationship between Ra_c and $\overline{S_{GD}}$; however, it clearly shows that the convective pattern selects a less irreversible path at each transition. Also plotted in figure 2 is a variation in the non-dimensional rate of entropy production per roll, $\overline{S_{GD}}/\hat{M}$ (dotted), with the aspect ratio, AR. Since the number of rolls increases by one as AR increases across a transition point, AR_{tran}, an abrupt drop in $\overline{S_{GD}}/\hat{M}$ occurs with the ratio of entropy generation per roll before and after a transition being equal to $(1 + 1/\hat{M})$. It is also noted that $\overline{S_{GD}}/\hat{M}$ is approximately 1.3 immediately after a transition to a higher number of rolls. It should be mentioned that the magnitudes of both $\overline{S_{GD}}$ and $\overline{S_{GD}}/\hat{M}$ are not affected significantly by a change in Ω.

The last quantity of interest useful for the present second-law analyses is the horizontal distribution of the rate of entropy generation in a cavity, $S'_G(x)$ [W m^{-1} K^{-1}]. Integrating the volumetric rate of entropy generation, (3), across the cavity height, we obtain

$$\overline{S'_G(x)} = \frac{\int_{-H/2}^{H/2} S'''_G \,\mathrm{d}y'}{(\Gamma / H)} = \overline{S'_{GB}(x)} + \overline{S'_{GH}(x)} + \overline{S'_{GV}(x)}, \tag{15}$$

where

$$\overline{S'_{GB}(x)} \quad \text{(due to base conduction)} = Ra_c^2,$$

$$\overline{S'_{GH}(x)} = \tfrac{1}{8}\pi^2 C'^2 \left[AR^2 + (\hat{k}^2 - AR^2)\cos^2(\tfrac{1}{2}\pi\hat{k}x)\right] \frac{Ra_c^2}{\hat{k}^2 + AR^2} \quad \text{for odd solutions;}$$

$$= \tfrac{1}{8}\pi^2 C'^2 \left[AR^2 + (\hat{l}^2 - AR^2)\sin^2(\tfrac{1}{2}\pi\hat{l}x)\right] \frac{Ra_c^2}{\hat{l}^2 + AR^2} \quad \text{for even solutions;}$$

$$\overline{S'_{GV}(x)} = \tfrac{1}{8}\pi^6 C'^2\, \Omega\, (\hat{k}^2 + AR^2) \left(\frac{4}{AR^2} + \frac{\hat{k}^4 - 6\hat{k}^2 AR^2 + AR^4}{\hat{k}^2 AR^4} \cos^2(\tfrac{1}{2}\pi\hat{k}x) \right)$$

for odd solutions;

$$= \tfrac{1}{8}\pi^6 C'^2\, \Omega\, (\hat{l}^2 + AR^2) \left(\frac{4}{AR^2} + \frac{\hat{l}^4 - 6\hat{l}^2 AR^2 + AR^4}{\hat{l}^2 AR^4} \sin^2(\tfrac{1}{2}\pi\hat{l}x) \right)$$

for even solutions.

In the equation above the last two terms, $\overline{S'_{GH}(x)}$ and $\overline{S'_{GV}(x)}$, respectively represent effects of heat transfer and dissipation by perturbations. At $AR = 1.2$, a single roll ($\hat{k} = 1$) being present in the cavity, $\overline{S'_{GH}(x)}$ shows a relatively uniform horizontal distribution. For $AR > 1$ the amplitude of $\cos^2(\frac{1}{2}\pi\hat{k}x)$ or $\sin^2(\frac{1}{2}\pi\hat{l}x)$ in $\overline{S'_{GH}(x)}$, $\hat{M}^2 - AR^2$ ($\hat{M} = \hat{k}$ *or* $\hat{l}$), is negative, implying that $\overline{S'_{GH}(x)}$ takes a maximum at

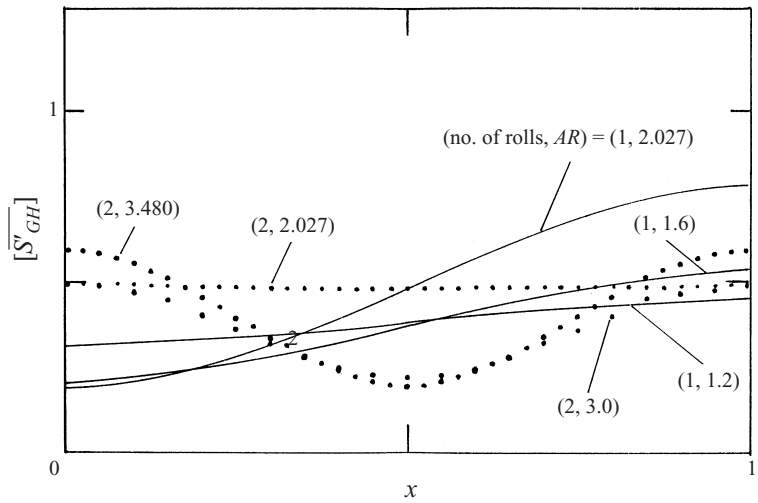

FIGURE 3. $[\overline{S'_{GH}(x)}]$ over a half-width for $\Omega = 10^3$ (free boundaries). Solid lines are for a single roll, dotted lines for two rolls in a cavity.

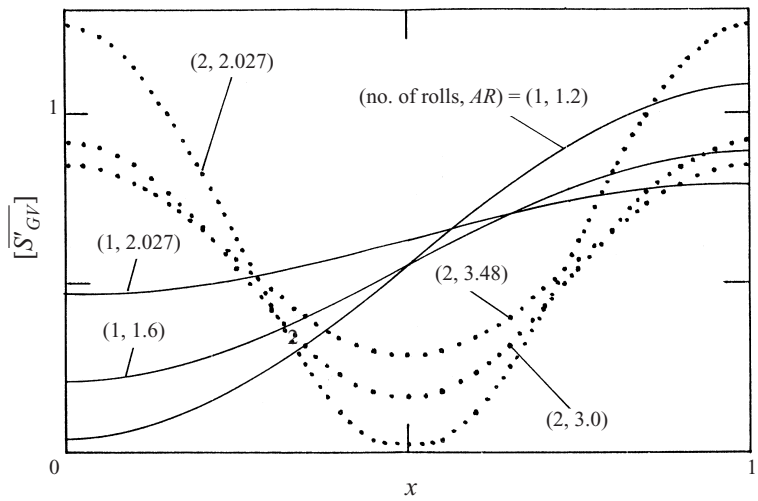

FIGURE 4. As figure 3 but for $[\overline{S'_{GV}(x)}]$.

the boundaries between two neighbouring rolls (including the sidewalls). Across a transition between an odd and an even number of rolls the amplitude of the x-direction variations of $\overline{S'_{GH}(x)}$ falls sharply as an exchange in amplitude between $(\hat{k}^2 - AR^2)$ and $(\hat{l}^2 - AR^2)$ occurs. On the other hand, the horizontal variations of $\overline{S'_{GV}(x)}$ is more complex as the numerator of the amplitude of $\cos^2(\frac{1}{2}\pi\hat{k}x)$ and $\sin^2(\frac{1}{2}\pi\hat{l}x)$, $\hat{M}^4 - 6\hat{M}^2AR^2 + AR^4$ ($\hat{M} = \hat{k}$ or $\hat{l}$), changes its sign at $AR/\hat{M} = (1+\sqrt{5}/3)^{1/2}$ (≈ 1.32) and $(1 - \sqrt{5}/3)^{1/2}$ (≈ 0.50). The second root, $AR/\hat{M} = (1 - \sqrt{5}/3)^{1/2}$, needs to be accounted for only when $\hat{k} = 1$. Figure 3 and Figure 4 are presented to illustrate the variations in the horizontal distributions of the rate of entropy generation over a half-width in a cavity. To present these figures, both $\overline{S'_{GH}(x)}$ and $\overline{S'_{GV}(x)}$ of (15) are divided by a characteristic value, which is defined as $\overline{S'_{GV}(x)}$ at $AR_c = \left(1 + \sqrt{5/3}\right)^{1/2} \hat{M}$.

At $AR = AR_c$, $\overline{S'_{GV}(x)}$ is constant.

The explicit forms of $\overline{[S'_{GH}(x)]}$ in figure 3 and $\overline{[S'_{GV}(x)]}$ in figure 4 are

$$\overline{[S'_{GH}(x)]} = \frac{AR_c^2\,[AR^2 + (\hat{M}^2 - AR^2)F(x)]\,Ra_c^2}{4\pi^4\,\Omega\,(\hat{M}^2 + AR_c^2)(\hat{M}^2 + AR^2)},$$

$$\overline{[S'_{GV}(x)]} = \frac{AR_c^2\,(\hat{M}^2 + AR^2)\,[4\hat{M}^2AR^2 + (\hat{M}^4 - 6\hat{M}^2AR^2 + AR^4)F(x)]}{4\,(\hat{M}^2 + AR_c^2)\,\hat{M}^2AR^4},$$

with

$$F(x) = \begin{cases} \cos^2(\frac{1}{2}\pi\hat{M}x) & \text{for a single roll} \\ \sin^2(\frac{1}{2}\pi\hat{M}x) & \text{for two rolls.} \end{cases}$$

To present figure 3, Ω is set to 10^3 to make the magnitude of $\overline{[S'_{GH}(x)]}$ an order of 0.1. At the transition from one to two rolls at $AR = 2.027$, $\overline{[S'_{GH}(x)]}$ of a single roll exhibits a large variation; while, the corresponding profile of two rolls is nearly uniform as shown in figure 3. On the other hand, the opposite is true for $\overline{[S'_{GV}(x)]}$ in figure 4. Before a transition the profile variation of the perturbation temperature field (i.e. $\overline{S'_{GH}(x)}$ is large, while after a transition the entropy production by the perturbation velocity field (i.e. $\overline{S'_{GV}(x)}$) varies greatly across the cavity since flow pattern changes across the transition.

4. Onset of instability in a cavity with rigid boundaries

A solution for rigid boundaries was first obtained by Kurzweg (1965) numerically through an application of the Galerkin method of weighted residuals. The trial functions, used by Kurzweg and employed also in the present study, are

$$\left.\begin{aligned} \Psi &= C_{o(e)} \sum_{m=1}^{M} \sum_{n=1}^{N} A_{mn}^{o(e)}\, F_m^{o(e)}(x) G_n^{o(e)}(y), \\ \theta &= C_{o(e)} \sum_{m=1}^{M} \sum_{n=1}^{N} B_{mn}^{o(e)}\, f_m^{o(e)}(x) g_n^{o(e)}(y), \end{aligned}\right\} \tag{16}$$

with o and e indicating an 'odd' and an 'even' solution respectively. The trial functions for Ψ are taken as eigenfunctions of the following eigenvalue problem:

$$\frac{\partial^4 \Psi}{\partial z^4} = \lambda^4\,\Psi, \qquad \psi = \partial\Psi/\partial z = 0 \quad \text{at} \quad z = \pm 1;$$

the trial functions for θ, on the other hand, is chosen in terms of sine and cosine functions. One of the advantages of the selection of the trial functions is that they satisfy the orthogonality properties, which make the ensuing application of the Galerkin method more effective. (For specific forms of $F_m^{o(e)}$ etc., see Kurzweg 1965.)

The solution obtained through an application of the Galerkin method with $M = N = 5$ (which results in a 50×50 determinant) is shown in figure 5. The present analysis shows an excellent agreement with the original analysis by Kurzweg (in which an 18×18 determinant is solved), predicting the transition in the number of rolls being at $AR_{tran} = 1.63$ (for 1 to 2 cells), 2.69 (2 to 3), 3.72 (3 to 4) and 4.76 (4 to 5).

The present analysis also predicts correctly a slow, consistent decrease of Ra_c with an increase in AR toward the limiting value of 1707.8 as $AR \to \infty$. Furthermore, an examination of the incipient rolls shows that the solution with $M = N = 5$ is

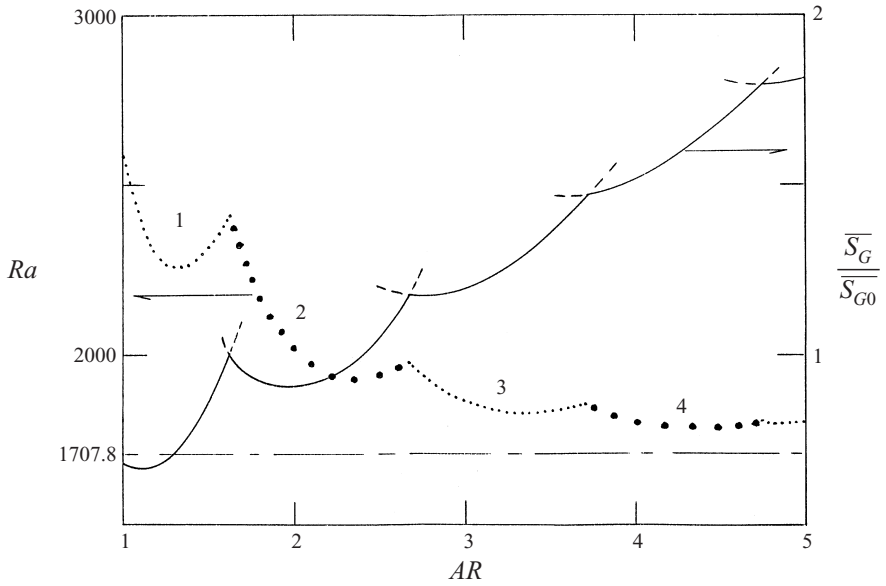

FIGURE 5. Linear stability in a cavity with rigid boundaries. $Ra_c, \overline{S_G}/\overline{S_{G0}}$ vs. AR with $\overline{S_{G0}} = \overline{S_G}$ of a single roll in a cavity at $AR = AR_{tran} = 1.63$. Small dots are for an odd number of rolls, large dots for an even number of rolls. Numbers above the curve represent the number of rolls in the cavity.

different from the corresponding solution with $M = N = 3$ by less than 0.5% in terms of the magnitude of Ψ at the horizontal midplane over the range of the present investigation ($\sim 1 < AR \lesssim 6$), indicating that the double-series expansion of (16) is effective in yielding a converged solution. Substantial differences in AR_{tran} between the case of the free and the rigid boundaries are due to the magnitude of the minimum horizontal wavenumber for the marginal stability. For a cavity with a large aspect ratio (or the Rayleigh–Bénard convection between two rigid horizontal boundaries) the width of a convective cell is equal to the distance between the two horizontal boundaries, forming a square cell. For the present case of a low aspect ratio cavity, the constraint imposed by the rigid sidewalls causes a difference in the horizontal size between the cells adjacent to and away from the sidewalls.

Substitution of θ and Ψ of (16) into the integral, $\langle\theta(-\partial\Psi/\partial x)\rangle$, which appears in (4), yields

$$\left\langle \theta\left(-\frac{\partial\Psi}{\partial x}\right)\right\rangle = C^2_{o(e)} \sum_{m=1}^{M}\sum_{n=1}^{N}\sum_{i=1}^{M}\sum_{j=1}^{N} A^{o(e)}_{mn}\, B^{o(e)}_{ij}\, \hat{I}^{o(e)}(i)\, F^{o(e)}(m, \hat{I}^{o(e)})\, G(n, \hat{J}), \quad (17)$$

where

$$\hat{I}^o(i) = \frac{2i-1}{2}\pi, \qquad \hat{I}^e(i) = -i\pi, \qquad \hat{J}(j) = \frac{2j-1}{2}\pi,$$

$$F^o(m, \hat{I}^o(i)) = \int_{-1}^{1} [\cosh(\lambda_m x)\cos(\hat{I}^o x) + q_m \cos(\lambda_m x)\cos(\hat{I}^o x)]\,\mathrm{d}x,$$

$$F^e(m, \hat{I}^e(i)) = \int_{-1}^{1} [\sinh(\tau_m x)\sin(-\hat{I}^e x) + r_m \sin(\tau_m x)\sin(-\hat{I}^e x)]\,\mathrm{d}x,$$

$$G(n, \hat{J}(j)) = \int_{-1}^{1} [\cosh(\lambda_n y)\cos(\hat{J} y) + q_n \cos(\lambda_n y)\cos(\hat{J} y)]\,\mathrm{d}y.$$

The integrals in the above equation may be readily obtained in explicit forms. The rate of entropy generation, $\overline{S_G}$, due to the perturbation fields is also plotted in figure 5. Compared to the case of free boundaries the rigid boundaries have a greater effect on the onset of instability as seen in the substantial variations both in the critical Rayleigh number and $\overline{S_G}$.

Finally the horizontal distribution of the rate of entropy generation in a cavity, $S'_G(x)$ [W m^{-1} K^{-1}] may be expressed as,

$$\overline{S'_G(x)} = \frac{\int_{-H/2}^{H/2} S'''_G \,\mathrm{d}y'}{(\Gamma / H)}$$

$$= \overline{S'_{GB}(x)} \text{ (due to base conduction)} + \overline{S'_{GH}(x)} \text{ (perturbed temperature effect)}$$

$$+\overline{S'_{GV}(x)} \text{ (perturbed velocity effect)}, \tag{18}$$

where

$$\overline{S'_{GB}(x)} = Ra_c^2,$$

$$\overline{S'_{GH}(x)} = \frac{C_{o(e)}^2 Ra_c^2}{2} \sum_{m=1}^{M}\sum_{n=1}^{N}\sum_{i=1}^{M}\sum_{j=1}^{N} B_{mn}^{o(e)} B_{ij}^{o(e)} \left[\frac{\mathrm{d}H_m^{o(e)}}{\mathrm{d}x}\frac{\mathrm{d}H_i^{o(e)}}{\mathrm{d}x} + AR^2 H_m^{o(e)} H_i^{o(e)} \left(\frac{2n-1}{2}\pi\right)\left(\frac{2j-1}{2}\pi\right)\right]\delta_{nj},$$

$$\overline{S'_{GV}(x)} = \frac{C_{o(e)}^2 \Omega}{2}\left(\frac{2}{AR}\right)^4 \sum_{m=1}^{M}\sum_{n=1}^{N}\sum_{i=1}^{M}\sum_{j=1}^{N} A_{mn}^{o(e)} A_{ij}^{o(e)} \times \left[4AR^2 \frac{\mathrm{d}F_m^{o(e)}}{\mathrm{d}x}\frac{\mathrm{d}Fi^{o(e)}}{\mathrm{d}x}\left\langle\left\langle \frac{\mathrm{d}G_n}{\mathrm{d}y}\frac{\mathrm{d}G_j}{\mathrm{d}y}\right\rangle\right\rangle + AR^4 F_m^{o(e)} F_i^{o(e)}\left\langle\left\langle \frac{\mathrm{d}^2G_n}{\mathrm{d}y^2}\frac{\mathrm{d}^2G_j}{\mathrm{d}y^2}\right\rangle\right\rangle - 2AR^2 \frac{\mathrm{d}^2F_m^{o(e)}}{\mathrm{d}x^2} F_i^{o(e)}\left\langle\left\langle G_n \frac{\mathrm{d}^2G_j}{\mathrm{d}y^2}\right\rangle\right\rangle + \frac{\mathrm{d}^2F_m^{o(e)}}{\mathrm{d}x^2}\frac{\mathrm{d}^2F_i^{o(e)}}{\mathrm{d}x^2}\langle\langle G_n G_j\rangle\rangle\right],$$

with $\langle\langle\, f(y)\,\rangle\rangle = \int_{-1}^{1} f(y)\,\mathrm{d}y$, δ_{nj} = the Kronecker delta,

$F_p^o\,(p = m \text{ or } i) = \cosh(\lambda_p x) + q_p \cos(\lambda_p x)$, $F_p^e\,(p = m \text{ or } i) = \sinh(\tau_p x) + r_p \cos(\tau_p x)$,

$$G_p\,(p = n \text{ or } j) = \cosh(\lambda_p y) + q_p \cos(\lambda_p y),\ H_p\,(p = m \text{ or } i) = \sin\left(\frac{2p-1}{2}\pi x\right).$$

Figures 6, 7 and 8 summarize the horizontal distributions of the rate of entropy generation as the number of convective rolls increases with AR. For $AR \leqslant 1.63$, a single roll occupies a cavity. (See figure 6.) As AR increases, $\overline{S'_{GH}(x)}$ becomes more uniform across the cavity. The distribution of $\overline{S'_{GV}(x)}$ is fairly even at $AR = 1$ except for a rise in its magnitude near the sidewall at $x = 1$. As AR increases $\overline{S'_{GV}(x)}$ decreases near the sidewall, indicating a weakening perturbation velocity field near the solid boundary. At $AR = 1.60$, slightly below the transition aspect ratio for the formation of two rolls, $\overline{S'_{GV}(x)}$ at the vertical boundary is very small. After a transition from a single roll to two rolls occupying the cavity at $AR = 1.63$, $\overline{S'_{GV}(x)}$ rises substantially

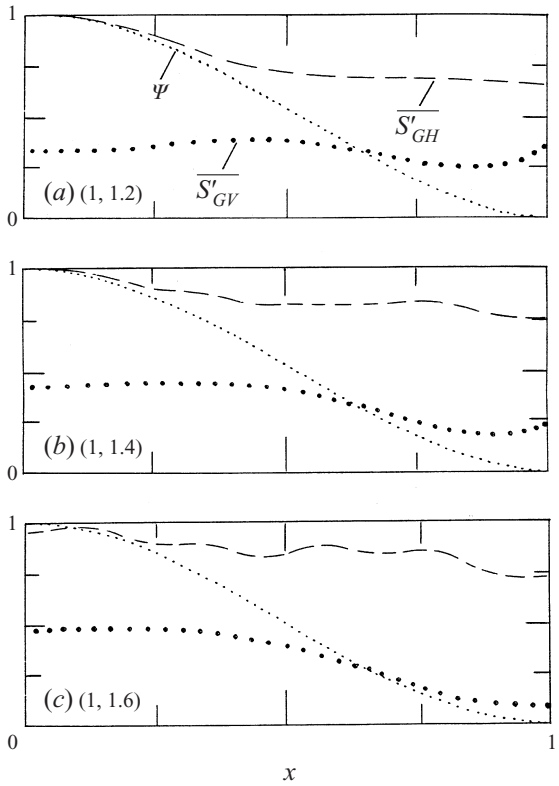

FIGURE 6. Profiles of Ψ at $y = 0$ (small dots), $\overline{S'_{GV}(x)}$ (large dots) and $\overline{S'_{GH}(x)}$ (broken) over a half-width (a single roll in a cavity with rigid boundaries). (All normalized with respect to their maximum values.) In the bracket (a, b), a = the number of rolls, b = AR.

near the sidewall; while $\overline{S'_{GH}(x)}$ decreases near $x = 0$ (the location of interface between the rolls) as well as near the sidewall. (See figure 7.) As AR increases beyond the transition aspect ratio of 1.63 $\overline{S'_{GH}(x)}$ increases near the cell boundary at $x = 0$, and decreases near the solid boundary with $\overline{S'_{GV}(x)}$ becoming very small again as AR approaches a transition to the formation of three rolls at $AR = 2.69$. Three rolls appear in the cavity for AR between 2.69 and 3.72. (See figure 8.) When more than two rolls occupy a cavity, the locations of the interface between rolls (i.e. the locations where the streamfunction at the horizontal midplane becomes zero) change as AR increases from a transition aspect ratio with the rolls in contact with the sidewalls increasing their horizontal size. Both $\overline{S'_{GH}(x)}$ and $\overline{S'_{GV}(x)}$ in the roll in contact with the vertical rigid boundary change their profiles with an increase in AR in a manner similar to the case of two rolls with very low value of $\overline{S'_{GV}(x)}$ near the sidewall as AR approaches the transition to four rolls at $AR = 3.72$. In the middle roll both $\overline{S'_{GH}(x)}$ and $\overline{S'_{GV}(x)}$ increases with AR, showing a nearly uniform profile at $AR = 3.70$.

5. Numerical analysis of supercritical state

To understand the entropy generation of natural convection in a rectangular cavity, numerical analyses are performed for natural convection in a rectangular cavity with

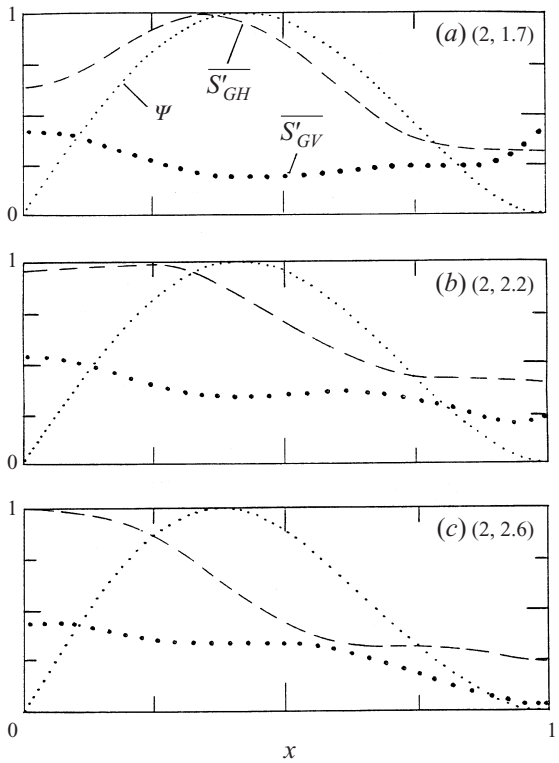

FIGURE 7. As figure 6 but showing two rolls in the cavity.

rigid boundaries and adiabatic sidewalls. Computational conditions are:

> nitrogen gas as the fluid (assuming an ideal gas with its density changes being directly related to temperature changes neglecting effects of small pressure changes around the specified pressure condition of $\sim$ 1 atm), $H = 1.58$ cm (fixed), range of $AR = 1$–2 (to examine the transition between one and two rolls), $T_2 = 300$ K (fixed), $Ra_c < Ra \lesssim 5000$ with the corresponding temperature difference, ΔT, of 5–15 K.

Thermophysical properties are evaluated at $(T_1 + T_2)/2$, and the computations are performed over the full width of the cavities. To solve a full set of steady, two-dimensional Navier–Stokes equations numerically along with the boundary conditions, the calculation domain is divided into a number of finite control volumes, and the conservation equations are integrated over each control volume. The set of discretized equations thus generated is based on a staggered grid system in which presssure and temperature are calculated at main grid points, while velocity components, u and v, are evaluated at secondary grid points. The grid system is based on variable spacing (min. 0.4 mm, max. 0.75 mm) with finer meshes near the boundaries. The convection–diffusion fluxes are evaluated by employing the 'hybrid' scheme. The mometum equations are solved using SIMPLER algorithm (Patankar 1980). A solution to a set of linear discretized equations is obtained by using the line-by-line TDMA (Tri-Diagonal Matrix Algorithm), followed by the evaluation of the entropy production rate through numerical integrations of velocity and temperature fields over the rectangular cross-section.

Figures 9–11 summarize the numerical results. In figure 9, in which temperature variations at the horizontal midplane are shown across the cavity width, a single roll

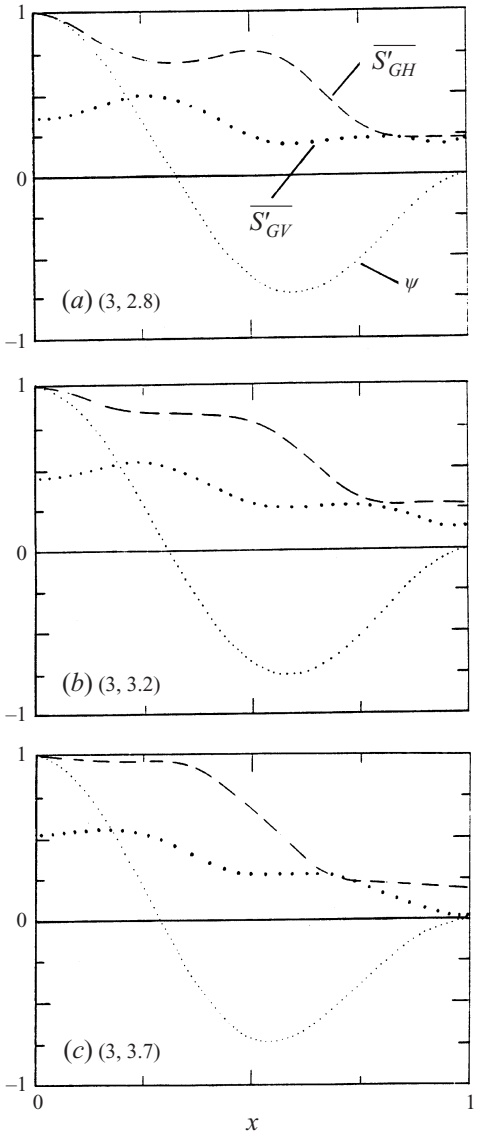

FIGURE 8. As figure 6 but showing three rolls in the cavity.

is present at $AR = 1.57$ for both cases of $Ra = 2800$ and 3780 as the flow circulating counterclockwise heats up the region near the right wall and cools the region near the left wall; while, both at $AR = 1.66, Ra = 2800$ and $AR = 1.59, Ra = 3780$, two counter-rotating rolls are present as the temperature profiles become nearly symmetric with respect to the vertical midplane. Shown in figure 10 is $\widehat{S'_G}$, (ratio of entropy generation by natural convection to that by the corresponding theoretical pure conduction at the same values of AR and ΔT), vs. AR for two Rayleigh numbers. The lower curve indicates a transition value of AR for $Ra = 2430$ close to the one predicted by stability analyses (figure 5) of $AR_{tran} = 1.63$ with $Ra_c = 2416$. On the other hand, at $Ra = 3780$ (upper curve) the transition (where an inflection occurs in

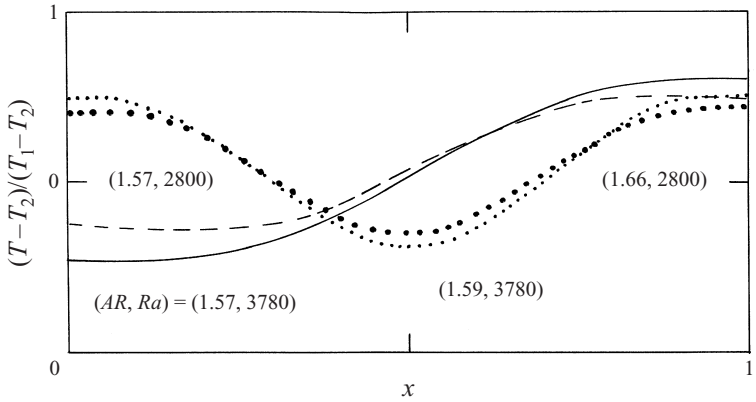

FIGURE 9. Temperature profiles at the horizontal midplane across the cavity.

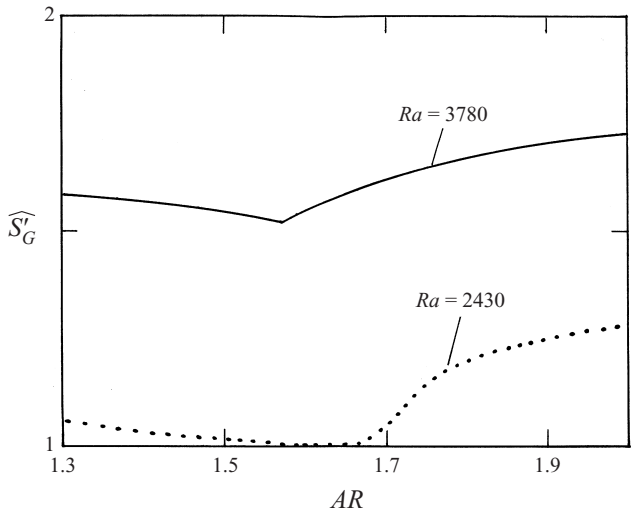

FIGURE 10. Rate of entropy generation (non-dimensional) in a cavity plotted against AR.

the curve) is at $AR \approx 1.58$, implying that the transition aspect ratio decereases with an increase in the Rayleigh number above Ra_c.

Figure 11 shows the development of the non-dimensional rate of entropy generation, $\widehat{S'_G}$, as Ra is increased. Noting again that the stability analysis yields the transition between one and two rolls at $AR = 1.63$ with $Ra_c = 2416$, the two curves with slightly different values of AR of 1.57 (one roll) and 1.66 (two rolls) merge to conduction states close to each other, indirectly supporting the imposed condition in our stability analyses that at the transition the magnitude of the entropy generation rate is the same for the odd solution and the even solution.

6. Summary and conclusion

The second law of thermodynamics is applied to natural convection in a rectangular cavity heated at the bottom and cooled at the top isothermally to obtain a general equation for the rate of entropy generation, which may be decomposed into two parts:

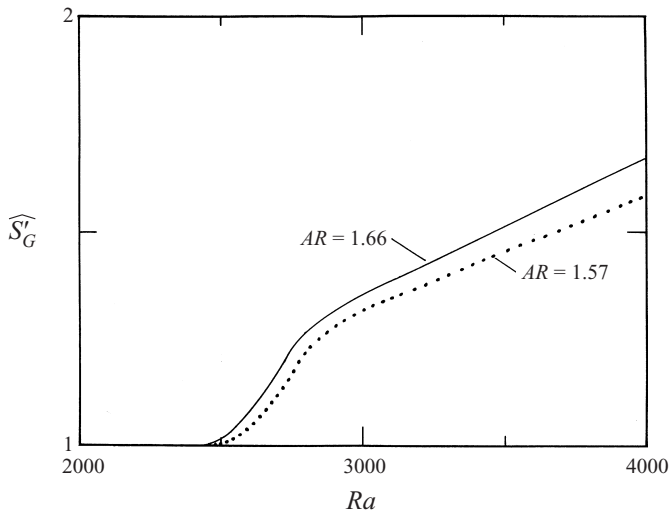

FIGURE 11. Increase in the rate of entropy generation (non-dimensional) in a cavity with Ra.

one due to thermal conduction and the other due to the net vertical advection of thermal energy. The conduction component is proportional to Ra^2, while the advection component is proportional to $(1 + \Omega/Ra)\,Ra^2$ with the ratio, Ω/Ra, indicating the relative importance of viscous friction and heat transfer in entropy generation. The result is then used to examine the linear stability for the onset of convective motion in a rectangular cavity, confirming the aspect ratio, AR_{tran}, where a transition in the number of convective rolls occurs, to be the state in which the incipient convective motion shifts to a different, less irreversible pattern. For the case of free boundaries the ratio of the entropy generation per roll across a transition aspect ratio is equal to $(1 + 1/\hat{M})$ when the number of rolls increases from $\hat{M}$ to $(\hat{M} + 1)$, and the rate of entropy generation per roll immediately after a transition is approximately constant and independent of the number of rolls present in the cavity. Distributions of entropy production rate between the part due to temperature perturbation and the part due to velocity perturbation are found to change drastically before and after a transition in the number of convective rolls. In contrast to the case of free boundaries, in which the thermofluid structure of a roll as well as the spatial distributions of the rate of entropy generation are the same among the rolls in a cavity, the rigid boundaries affect the entropy distributions between rolls substantially. The present analysis shows that a transition into a higher number of convective rolls is associated with an abrupt change in the rate of entropy generation by the perturbation velocity field near the vertical rigid boundaries. Also, a substantial profile change (both in $\overline{S'_{GH}(x)}$ and $\overline{S'_{GV}(x)}$) across a roll in contact with a sidewall implies that a transition in the convective pattern is closely related to the thermofluid structure of the rolls in contact with vertical boundaries.

In many scientific and engineering problems such as heat transfer by natural convection in a cavity and mixed (combined forced and natural) convection in a duct or in a chamber for chemical vapour deposition processes, thermal (temperature) and hydrodynamic (velocity) fields need to be examined carefully to understand the overall transport process. The present study suggests an advantage of employing the second-law analysis as both temperature and velocity fields may be examined simultaneously in terms of the entropy generation.

REFERENCES

Bejan, A. 1982 *Entropy Generation Through Heat and Fluid Flow*. John Wiley and Sons.

Davis, S. H. 1967 Convection in a box: linear theory. *J. Fluid Mech.* **30**, 465–478.

Gebhart, B., Jaluria, Y., Mahajan, R. L. & Sammakia, B. 1988 *Buoyancy-Induced Flows and Transport*. Hemisphere.

Kurzweg, U. H. 1965 Convective instability of a hydromagnetic fluid within a rectangular cavity. *Intl J. Heat Mass Transfer* **8**, 35–41.

Patankar, S. V. 1980 *Numerical Heat Transfer & Fluid Flow*. Hemisphere.

Turner, J. S. 1973 *Buoyancy Effects in Fluids*. Cambridge University Press.

Zimmermann, W. 1991 *Pattern Formation in Electro-Hydrodynamic Convection*. MRS Bulletin, XVI, 46–56.